C. R. Mecanique 342 (2014) 376–381

Contents lists available at ScienceDirect

Comptes Rendus Mecanique

www.sciencedirect.com

Separation flow control

Flow control on a 3D backward facing ramp by pulsed jets

Contrôle d'écoulemement dans le sillage d'une rampe descendante 3D par jets pulsés

Pierric Joseph [a,*], Dorian Bortolus [a], Francesco Grasso [a,b]

[a] *Institut aérotechnique (IAT–CNAM), 15, rue Marat, 78210 Saint-Cyr-l'École, France*
[b] *CNAM, Laboratoire DynFluid, 151, boulevard de l'Hôpital, 75013 Paris, France*

ARTICLE INFO

Article history:
Received 26 July 2013
Accepted 14 December 2013
Available online 21 June 2014

Keywords:
Flow control
Pulsed jets
Backward facing ramp
PIV

Mots-clés :
Contrôle d'écoulemement
Jets pulsés
Rampe descendante

ABSTRACT

This paper presents an experimental study of flow separation control over a 3D backward facing ramp by means of pulsed jets. Such geometry has been selected to reproduce flow phenomena of interest for the automotive industry. The base flow has been characterised using PIV and pressure measurements. The results show that the classical notchback topology is correctly reproduced. A control system based on magnetic valves has been used to produce the pulsed jets whose properties have been characterised by hot wire anemometry. In order to shed some light on the role of the different parameters affecting the suppression of the slant recirculation area, a parametric study has been carried out by varying the frequency and the momentum coefficient of the jets for several Reynolds numbers.

RÉSUMÉ

Ce travail présente une étude expérimentale du contrôle d'un décollement dans le sillage d'une rampe descendante 3D par jets pulsés. Cette géométrie a été choisie pour reproduire un écoulement d'intérêt pour l'industrie automobile. L'écoulement de base a été caractérisé par PIV et mesures de pression. Les résultats montrent que la topologie de type tricorps est correctement reproduite. Un système de contrôle basé sur des électrovannes a été utilisé pour créer les jets pulsés, dont les propriétés ont été caractérisées par anémométrie à fil chaud. Afin d'éclairer le rôle des paramètres affectant la suppression de la zone décollée, une étude paramétrique a été menée en changeant la fréquence et la quantité de mouvement injectée pour différents nombres de Reynolds.

* Corresponding author.
E-mail address: pierric.joseph@cnam.fr (P. Joseph).

http://dx.doi.org/10.1016/j.crme.2013.12.010
1631-0721/

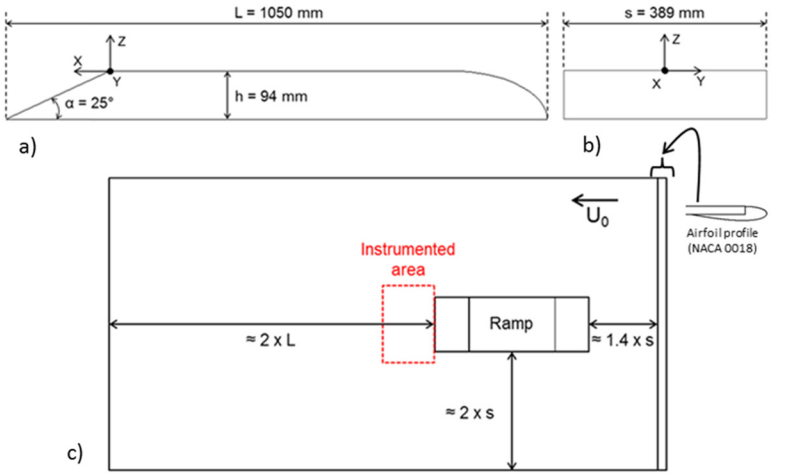

Fig. 1. (Colour online.) Side (a) and front (b) views of the backward facing ramp; (c) top view of the elevated floor with model arrangement.

1. Introduction

1.1. Context

Today environmental issues demand a drastic reduction of both pollutants emissions and fuel consumption. These issues are of great importance for the transport industry, especially for automotive manufacturers. When considering high speed displacements like highway travelling, drag reduction with the constraints of security and design is indeed one of the main concerns of the automotive industry. Active flow control, relying on an external energy source, has been shown to be an effective means to modify the flow around various bodies [1], including automotive shapes. Different techniques can be found in the literature, like moving walls [2], plasma actuators [3], or the ones based on the use of jets. Continuous blowing or suction has been applied for a long time in aeronautics [4], and both are studied for automotive applications [5,6]. Periodic blowing (either pulsed or synthetic jets) appears to be a much more efficient solution [7] at the cost of a greater complexity. Even though the technic is successfully applied in automotive related studies [8–10], it needs to be further investigated, especially to optimise the efficiency of the control action in full 3D cases with finite spanwise (which are closer to the industrial cases).

In the present work, we have carried out an experimental study of flow separation control over a 3D backward facing ramp by means of pulsed jets. Such geometry has been selected to reproduce flow phenomena of interest for the automotive industry. In the following, we first characterise the base flow through PIV and pressure measurements. We then describe the control system and characterise the properties of the pulsed jets by hot wire anemometry. Finally, we present results of flow control through a parametric study whereby the frequency and the momentum coefficient of the jets were varied for several Reynolds numbers.

1.2. Experimental setup

Experiments were carried out in the S4 wind tunnel of the Institut aérotechnique (IAT–CNAM, France). The S4 test cross section is 5 m × 3 m, and the flow velocity (U_0) ranges from 20 m s^{-1} to 40 m s^{-1} with a maximum turbulent intensity of 1.2%. The model geometry is depicted in Fig. 1 (observe that all dimensions are in millimetres). In order to minimise the effect of the boundary layer developing on the floor of the tunnel, the ramp lays on an elevated floor (see Fig. 1c) with an airfoil-shaped leading edge to prevent separation. This elevated floor presents an instrumented area as flow structures expands farther in the wake.

With this arrangement, upstream of the separation point the boundary layer thickness is $\delta_{99} = 27 \times 10^{-3}$ m (measurements carried out with total pressure probe at $X = -5 \times 10^{-2}$ m, $Y = 9.5 \times 10^{-2}$ m). Oil flow visualisation of the base flow (discussed in the next section) confirmed that the flow is symmetric on average. Therefore, only half of the rear part of the model (both the slant and the instrumented area of the elevated floor) was instrumented with 141 pressure taps. Wall pressure measurements were obtained by using a scanivalve pressure scanner (accuracy: 0.03%), and the results are expressed in terms of the pressure coefficient $C_p = (p - p_0)/(\frac{1}{2}\varrho U_0^2)$, where p and p_0 are, respectively, the local and undisturbed static pressure, and $\frac{1}{2}\varrho U_0^2$ is the dynamic pressure. PIV measurements were realised using an Nd:YAG laser (200 mJ, 15 Hz) and a FlowSense EO 4M camera. Oil droplets (average size: 2 µm) were used to seed the flow. The velocity field was characterised both in the streamwise (XZ) and spanwise (YZ) directions; the dimensions of the measurement planes are: 0.56 m × 0.56 m in the XZ plane, and 0.46 m × 0.46 m in the YZ plane, with 2048 × 2048 pixels resolution. The velocity

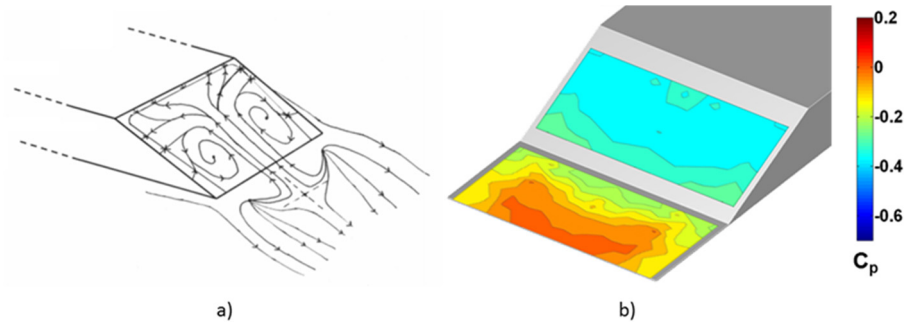

Fig. 2. (Colour online.) Base flow. Friction lines interpreted from oil flow visualisations (a) and pressure coefficient distribution (b). $\mathrm{Re}_L = 1.4 \times 10^6$.

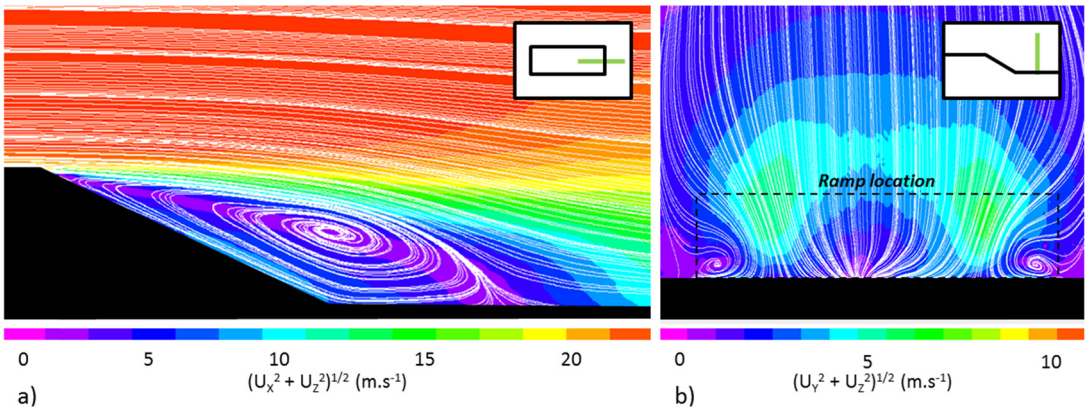

Fig. 3. (Colour online.) Streamlines and contours of velocity module reconstructed through PIV measurements in the longitudinal (a: $Y = 0$) and transversal plane (b: $X = 0.124$ m). $Re_{\mathrm{L}} = 1.4 \times 10^6$.

is calculated by using an adaptive correlation algorithm, with a final interrogation size of 16×16 pixels with 50% overlap. A minimum of 800 pairs of images are realised for each measurement planes.

2. Study of the base flow

The base flow was first investigated by means of oil flow visualisation by using a special mixture of dodecan, silicon oil, oleic acid, and titanium oxide, in various proportions. This mixture was applied on the slanted surface, thus allowing visualisation of friction lines when the model is exposed to an air flow. The flow topology reconstructed through the friction lines is shown in Fig. 2a for $Re_{\mathrm{L}} = \varrho U_0 L/\mu = 1.4 \times 10^6$. The figure highlights that the flow separates immediately after the slant edge, and reattaches further on the elevated floor. The reattachment point on the mid-plane coincides with the saddle point clearly visible in the figure. On the slant surface, the back flow rolls up around two foci points, indicating the birth of longitudinal flow structures. This mean flow topology is consistent with the one existing on the rear window of the notchback vehicle as, for example, the one described by Gilhome et al. [11]. In Fig. 2b, we have also reported the C_p distribution on both the slant and the flat surface. The figure shows that the flow undergoes a pressure decrease on the slant surface, consistent with a detached zone, and a progressive pressure recovery further downstream in the wake. The reattachment line is clearly visible past the foot of the slant, and the mean flow topology is confirmed by the pressure contours.

In order to characterise the recirculation bubble and the longitudinal flow structures, PIV measurements were carried out in both longitudinal ($Y = 0$) and transversal planes ($X = 0.124$ m) at various Reynolds numbers (only the results for $Re_{\mathrm{L}} = 1.4 \times 10^6$ are reported in Fig. 3). In the spanwise direction (Fig. 3a), the streamlines roll up, giving rise to a recirculation bubble with a low velocity area. The estimated recirculation extent is approximately equal to 0.26 m and is rather independent of the Reynolds number. In the streamwise direction (Fig. 3b), the roll up of the streamlines indicates the occurrence of two longitudinal structures, and the associated inflow is clearly visible from the velocity contours.

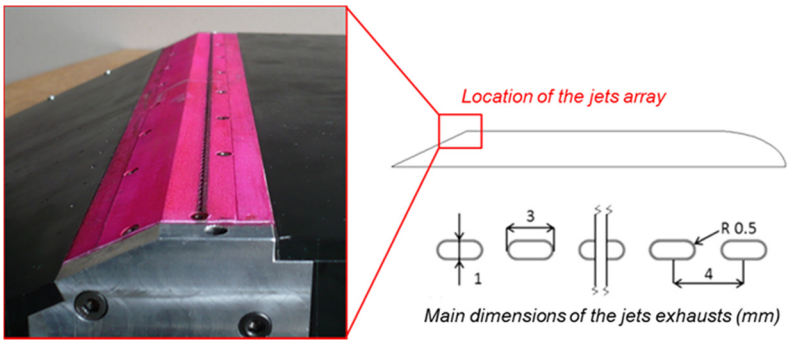

Fig. 4. (Colour online.) Location of the jets and main dimensions of the exhaust orifices (in mm).

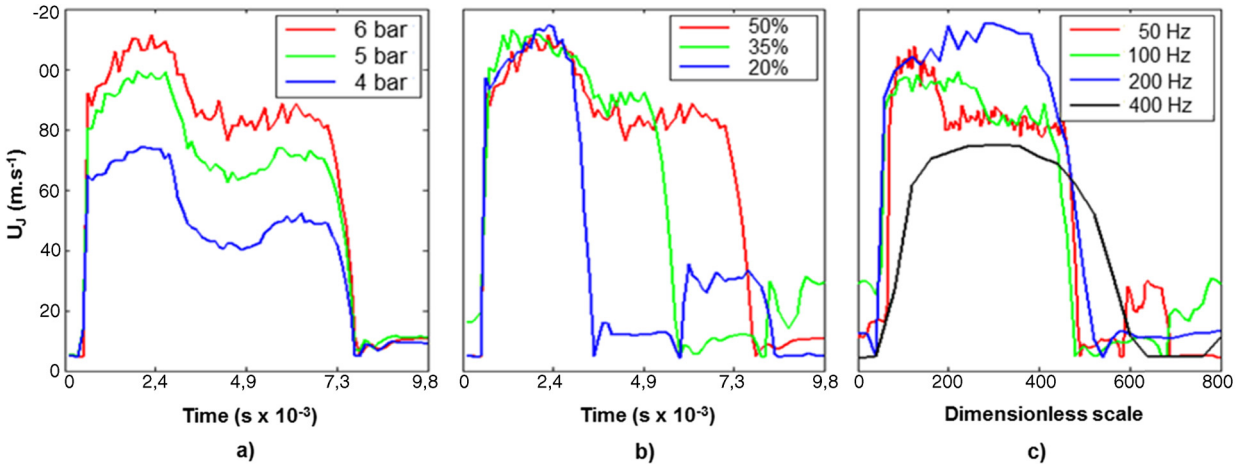

Fig. 5. (Colour online.) Time history of the jet velocity for various supply pressures (a: $f_J = 70$ Hz, DC = 50%), for various duty cycles (b: $p_S = 6$ bar, $f_J = 70$ Hz) and for various frequencies (c: $p_S = 6$ bar, DC = 50%).

3. Flow control system

3.1. Description of the control system and of the actuators

The flow control strategy relies on pulsed jets produced by magnetic valves, as described in references [9,12]. The jets exhaust through a discontinuous slot made out of 89 rectangular orifices located 10 mm upstream of the slant edge (see Fig. 4). This configuration produces longitudinal vorticity generated through a pair of counter rotating vortices created by each jet [9,12].

Actuators are magnetic valves (Matrix Ltd.) with an operating frequency up to $f_J = 500$ Hz and operating supply pressure (p_S) up to 8 bar. Valves are fed by a pressure supplier and they are driven by a specific electronic card (both for electrical supply and frequency command signal). They are connected to a specific cavity filled with glass micro-balls that ensure the homogeneity of the air flow through the jets array (for more technical details, see reference [12]). A square wave oscillating between 0 and 5 volts with variable frequency and variable duty cycle drives the control system.

3.2. Characterisation of the jets

In order to understand the effect of flow control, it is important to have a good knowledge of the injected perturbation whose spatio-temporal characteristics strongly depend on the actuator and on the command parameters. For example, the time history of the jet velocity can be strongly affected by design limitations of the actuators. We have then characterised the jet velocity (U_J) as a function of the supply pressure, duty cycle (DC) and command frequency by means of a single-component hot-wire anemometer. The probe was located 1 mm above the exhaust orifice and the jet velocity was recorded for a period of 5 s with a sample frequency of 8192 Hz. The time history of U_J is reported in Fig. 5 for various supply pressures, duty cycles, and command frequencies.

Fig. 5a shows that U_J increases with the supply pressure p_S (and hence with the flow rate). One can also observe that the velocity of the jet exhibits a significant overshoot at the beginning of the blowing phase. This phenomenon is most likely due to a rapid release of the supply pressure associated with the actuator technology [13]. When varying the

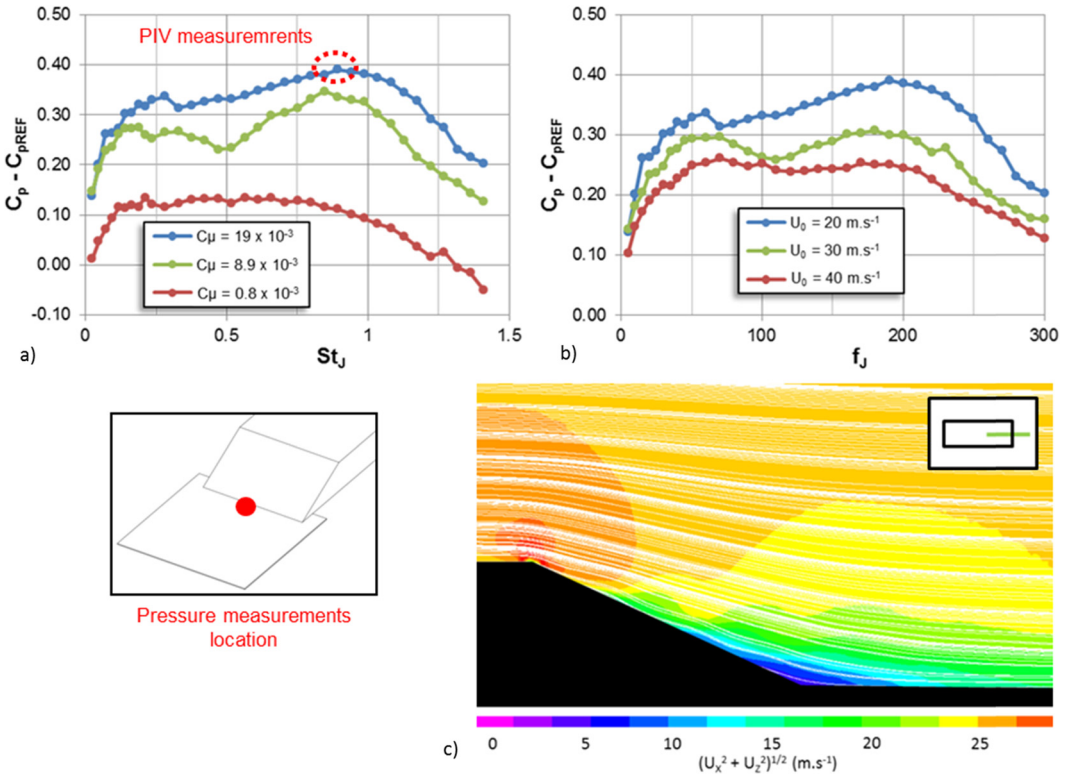

Fig. 6. (Colour online.) Flow control. Distribution of the pressure coefficient (6a, 6b) for various momentum coefficients and flow velocities; streamlines and contours of the velocity module (6c) reconstructed through PIV measurements in the longitudinal plane ($Y = 0$) for $C\mu = 19 \times 10^{-3}$, $St_J = 0.89$ and $Re_L = 1.4 \times 10^6$.

duty cycle (Fig. 5b), for a fixed frequency and supply pressure, the overshoot phase remains unaffected and the low-speed phase is reduced. A similar phenomenon is observed when changing the jet frequency (Fig. 5c). At low frequency, both phases (overshoot and low speed) are present, while at higher frequency only the overshoot phase remains. However, at frequencies greater than 300 Hz, the opening duration of the valve is not sufficient to ensure the establishment of the jet, and its velocity is greatly reduced.

4. Flow control

A parametric study was carried out by varying the frequency of the jets, the injected momentum and the flow velocity. Let $C\mu$ be the momentum coefficient defined as $C\mu = \varrho S_J U_{JM}^2/(\frac{1}{2}\varrho S_0 U_0^2)$ where U_{JM}, S_J, and S_0 are, respectively, the mean velocity of the jets, the total surface of the cross section of the orifices and the model cross section. For a fixed duty cycle (DC = 50%), three values of $C\mu$ were considered ($C\mu = 0.8 \times 10^{-3}$, 8.9×10^{-3} and 19×10^{-3}) and the frequency was varied between 5 and 300 Hz. The influence of the flow velocity was also analysed by considering three different values ($U_0 = 20$ m s^{-1}, 30 m s^{-1}, and 40 m s^{-1}). Fig. 6 shows the distribution of the pressure recovery in the presence of flow control (i.e. the variation of the pressure coefficient with respect to the uncontrolled flow) as a function of the reduced frequency of the jet St_J ($St_J = f_J h/U_0$), h being the height of the ramp, see Fig. 1.

As already found by Joseph et al. [12], Fig. 6a shows that the pressure recovery increases with the injected momentum. For low values of injected momentum, the response of the flow to the actuation is rather limited and it is insensitive to the actuation frequency. For higher values of $C\mu$, the flow seems to respond to two distinct "optimal" frequencies corresponding to $St_J = 0.28$ ($f_J = 60$ Hz) and $St_J = 0.89$ ($f_J = 190$ Hz). The streamlines and contours of velocity module reconstructed through PIV measurements in the longitudinal plane ($Y = 0$) are reported in Fig. 6c for $C\mu = 19 \times 10^{-3}$, $St_J = 0.89$ and $Re_L = 1.4 \times 10^6$. The figure shows that the recirculation area is indeed completely suppressed by the control action.

The analysis of the response of the flow to the actuation frequency as a function of the flow velocity (Fig. 6b) shows that these "optimal" control frequencies do not depend on U_0. These results seem to show that the most effective control frequencies are not linked to flow instabilities (whose natural frequencies are expected to evolve with the flow velocity), but depend on a mechanism associated with the actuator.

Fig. 7a depicts the pressure coefficient distribution for $C\mu = 19 \times 10^{-3}$, $St_J = 0.89$ and $Re_L = 1.4 \times 10^6$. One can observe that the suppression of the recirculation area is associated with a global pressure recovery almost everywhere on the rear part of the model. In the presence of control, very low pressure levels are also induced near the lateral slant edges. PIV

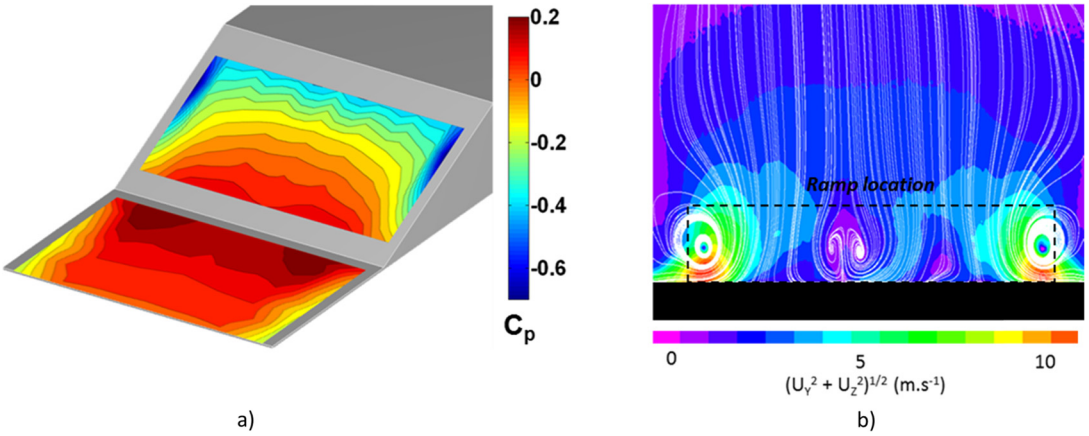

Fig. 7. (Colour online.) Flow control. Streamlines and contours of velocity module (7a) reconstructed through PIV measurements in the transversal plane ($X = 0.124$ m) and distribution of the pressure coefficient (7b) for $C\mu = 19 \times 10^{-3}$, $St_J = 0.89$ and $Re_L = 1.4 \times 10^6$.

measurements in the transversal plane and for the same values of $C\mu$, St_J and Re_L show that longitudinal flow structures have been strengthened (Fig. 7b). This phenomenon is likely to be responsible for the reinforcement of the side effect observed on the pressure distribution as also already highlighted by other authors [12,14], and that is expected to decrease the control performance.

5. Conclusions and perspectives

In the present paper, some experimental results of active flow control on a 3D backward facing ramp have been discussed with application to automotive flows. The analysis relies on the use of pressure and PIV measurements and of hot-wire anemometry. The injected perturbation produced by pulsed jets has been first characterised, and some particular features have been highlighted, such as the significant overshoot at the opening of the valve. A parametric study has been carried out by varying the frequency of the actuator, the injected momentum and the flow velocity of the experiment. The results seem to indicate that the interaction with flow instabilities is rather weak and the flow is likely to respond to a mechanism associated with the actuator. In line with the conclusion of reference [15], the global functioning mode of the selected strategy appears to be similar to dynamic vortex generators. In order to optimise the efficiency of the control system, the reattachment process will be investigated in future work by using unsteady measurement techniques. In order to quantify the influence of the reinforcement of the longitudinal structures, an evaluation of the drag force using detailed flow measurements (velocity and pressure fields) is also planned.

References

[1] M. Gad-el-Hak, Flow Control: Passive, Active, and Reactive Flow Management, Cambridge University Press, Cambridge, UK, 2000.
[2] J.-F. Beaudoin, O. Cadot, J.-L. Aider, J.E. Wesfreid, Bluff-body drag reduction by extremum-seeking control, J. Fluids Struct. 22 (6–7) (2006) 973–978.
[3] V. Boucinha, R. Weber, A. Kourta, Drag reduction of a 3D bluff body using plasma actuators, Int. J. Aerodyn. 1 (3/4) (2011) 262–281.
[4] S.F. Hoerner, Fluid-Dynamic Lift: Practical Information on Aerodynamic and Hydrodynamic Lift, Hoerner Fluid Dynamics, New York, 1992.
[5] S. Aubrun, J. McNally, F. Alvi, A. Kourta, Separation flow control on a generic ground vehicle using steady microjet arrays, Exp. Fluids 51 (5) (2011) 1177–1187.
[6] R.P. Littlewood, M.A. Passmore, Aerodynamic drag reduction of a simplified squareback vehicle using steady blowing, Exp. Fluids 53 (2) (2012) 519–529.
[7] D. Greenblatt, I. Wygnanski, The control of flow separation by periodic excitation, Prog. Aerosp. Sci. 36 (7) (2000) 487–545.
[8] S. Krajnović, J. Fernandes, Numerical simulation of the flow around a simplified vehicle model with active flow control, Int. J. Heat Fluid Flow 32 (1) (2011) 192–200.
[9] P. Joseph, X. Amandolese, C. Édouard, J.-L. Aider, Flow control using MEMS pulsed micro-jets on the Ahmed body, Exp. Fluids 54 (1) (2013) 1–12.
[10] A. Kourta, C. Leclerc, Characterization of synthetic jet actuation with application to Ahmed body wake, Sens. Actuators A, Phys. 192 (0) (2013) 13–26.
[11] B. Gilhome, J. Saunders, J. Sheridan, Time averaged and unsteady near-wake analysis of cars, SAE technical paper 2001-01-1040, 2001.
[12] P. Joseph, X. Amandolèse, J.-L. Aider, Drag reduction on the 25° slant angle Ahmed reference body using pulsed jets, in: 47th Symposium of Applied Aerodynamics, 3AF, Paris, France, 2012, p. 10.
[13] C. Braud, A. Dyment, P. Dupont, J. Foucaut, M. Stanislas, Development of a new system to generate pulsed-jets for turbulent flow separation control (macro-scale), in: Contrôle des décollements, vol. 2, GDR 2502, 2009, pp. 167–176.
[14] M. Rouméas, P. Gilliéron, A. Kourta, Drag reduction by flow separation control on a car after body, Int. J. Numer. Methods Fluids 60 (11) (2008) 1222–1240.
[15] J. Ortmanns, M. Bitter, C.J. Kähler, Dynamic vortex structures for flow-control applications, Exp. Fluids 44 (3) (2008) 397–408.